https://doi.org/10.1093/plphys/kiac215 PLANT PHYSIOLOGY 2022: 189: 2281–2297

Plant Physiology®

Research Article

A PLETHORA/PIN-FORMED/auxin network mediates prehaustorium formation in the parasitic plant *Striga hermonthica*

Ting Ting Xiao ,[1] **Gwendolyn K. Kirschner** ,[1] **Boubacar A. Kountche** ,[2] **Muhammad Jamil** ,[2] **Maria Savina** ,[3,4] **Vinicius Lube** ,[1] **Victoria Mironova** ,[5] **Salim al Babili** [2] **and Ikram Blilou** [1,*,†]

1 BESE Division, Plant Cell and Developmental Biology, King Abdullah University of Science and Technology, Thuwal, Kingdom of Saudi Arabia
2 BESE Division, The BioActives Lab, King Abdullah University of Science and Technology, Thuwal, Kingdom of Saudi Arabia
3 Institute of Cytology and Genetics, Novosibirsk 630090, Russian Federation, Russia
4 Novosibirsk State University, Novosibirsk 630090, Russian Federation, Russia
5 Plant Systems Physiology, Radboud University, 6500 AJ Nijmegen, the Netherlands

*Author for correspondence: Ikram.blilou@kaust.edu.sa
†Senior author

The study was conceptualized by I.B. The experimental designs were developed by I.B., T.T.X., and S.B. T.T.X. and G.K.K. analyzed the Striga root anatomy and cell division rates. T.T.X. performed in situ hybridization and immunolocalization. B.A.K., M.J., and S.B. contributed in the design of the auxin experiment, provided Striga seeds, helped with the sterilization and plant materials, and instructed T.T.X. and G.K.K. in handling Striga plants. V.L. performed macro-Striga images and edited movies from time-lapse imaging. V.M. and S.M. performed mathematical modeling. All authors contributed to discussing the results of this manuscript.
The author responsible for distribution of materials integral to the findings presented in this article in accordance with the policy described in the Instructions for Authors (https://academic.oup.com/plphys/pages/general-instructions) is: Ikram Blilou (Ikram.blilou@kaust.edu.sa).

Abstract

The parasitic plant Striga (*Striga hermonthica*) invades the host root through the formation of a haustorium and has detrimental impacts on cereal crops. The haustorium results from the prehaustorium, which is derived directly from the differentiation of the Striga radicle. The molecular mechanisms leading to radicle differentiation shortly after germination remain unclear. In this study, we determined the developmental programs that regulate terminal prehaustorium formation in *S. hermonthica* at cellular resolution. We showed that shortly after germination, cells in the root meristem undergo multiplanar divisions. During growth, the meristematic activity declines and associates with reduced expression of the stem cell regulator *PLETHORA1* and the cell cycle genes *CYCLINB1* and *HISTONE H4*. We also observed a basal localization of the PIN-FORMED (PIN) proteins and a decrease in auxin levels in the meristem. Using the structural layout of the root meristem and the polarity of outer-membrane PIN proteins, we constructed a mathematical model of auxin transport that explains the auxin distribution patterns observed during *S. hermonthica* root growth. Our results reveal a fundamental molecular and cellular framework governing the switch of *S. hermonthica* roots to form the invasive prehaustoria.

Introduction

The parasitic plant Striga (*Striga hermonthica*), commonly known as purple witchweed, is an obligate root hemiparasite belonging to the Orobanchaceae family that causes massive yield losses in agronomically important cereal crops such as sorghum (*Sorghum bicolor*), maize (*Zea mays*), and millet

Received August 31, 2021. Accepted March 25, 2022. Advance access publication May 11, 2022

(*Pennisetum glaucum*). It is considered a major threat to global food security (Pennisi, 2015), particularly in sub-Saharan Africa (Ejeta, 2007; Kountche et al., 2016). Striga seeds can only germinate in close proximity to the host roots as they depend on stimulants, mainly strigolactones produced by the host roots (Cook et al., 1972; Al-Babili and Bouwmeester, 2015). Striga sp. invades its host by forming a hairy structure that is central to successful invasion. This structure has been given different terminologies that are: "early haustorial", "proto-haustorium", "pre-attachment haustorium", and "prehaustorium" (reviewed in Furuta et al., 2021). In this study, we use the term "prehaustorium" to define the stage prior to the attachment to the host plant and the "invading haustorium" as the stage where the Striga roots produce invasive cells that start invading the host (Furuta et al., 2021). Successful invasion by the prehaustorium leads to the formation of the haustorium that connects the Striga root to the host through the vasculature (Raghavan and Okonkwo, 1982; Hood et al., 1998). Members of the Orobanchaceae family employ two types of haustoria: a primary/terminal haustorium that develops from the differentiation of the root meristem shortly after germination and a lateral haustorium that emerges from the de-differentiation of cells from the cortex, similar to *de novo* organ formation, such as in lateral roots or root nodules (Joel and Losner-Goshen, 1994; Goyet et al., 2019).

The initiation of the prehaustorium requires host-derived molecules from plant root exudates known as haustorium-inducing factors (HIFs). One of the commonly used HIF is the quinone 2,6-dimethoxy-1,4-benzoquinone, DMBQ (Chang and Lynn, 1986), a metabolite that results from lignin degradation and biosynthesis (Westwood et al., 2010) and is recognized by leucine-rich repeat receptor-like kinases in the hemiparasite *Phtheirospermum japonicum* (Laohavisit et al., 2020). The prehaustorium invades the host by applying mechanical pressure to the host cells in combination with enzymatic secretion, thereby allowing the invading haustorium to enter the intercellular space and colonize the host root (Perez-de-Luque, 2013). The haustorium is then established by forming a vascular connection with the host to acquire water and nutrient. This structure, enables the parasite to grow and proliferate at the expense of the host (Yoshida et al., 2016). The establishment of the xylem bridge that connects the parasite to the host is mediated by polar auxin transport; the PIN-FORMED (PIN) proteins, which are efflux carriers, play a major role in this process (Wakatake et al., 2020). Furthermore, the auxin biosynthesis gene *YUCCA3* has been found to be essential for lateral haustorium formation in *P. japonicum* (Ishida et al., 2016).

The process of lateral haustorium formation in the facultative parasite *P. japonicum* has been extensively studied, and the mechanisms underlying its development are slowly emerging owing to the availability of genetic tools and cell type-specific reporters. The lack of these tools in other parasitic species hampers advancement in the understanding of the developmental programs underlying the formation of the haustoria. Nevertheless, comprehensive transcriptome analysis of Striga roots from germination to haustorium formation has revealed the differential expression of developmental genes at the early stages, followed by an increase in the expression level of auxin transport and response genes (Yoshida et al., 2019). Despite these recent advances, a comprehensive analysis of the cellular and molecular morphodynamics of Striga roots that lead to terminal haustorium formation is still lacking.

In this study, we describe the development of the prehaustorium that will lead to the formation of the terminal haustorium in *S. hermonthica* and provide insights into the mechanisms underlying its morphodynamics during growth. We showed that after germination, *S. hermonthica* develops a root meristem with an anatomy that resembles that of the model plant Arabidopsis (*Arabidopsis thaliana*) (Raghavan and Okonkwo, 1982; Hood et al., 1998). We marked the stem cell niche of the Striga root using the stem cell regulator *PLETHORA1* (*PLT1*) and defined the cellular organization of the Striga root meristem. Using cell cycle markers, we found that at early stages, the meristematic cells undergo multiplanar cell divisions. These divisions decrease at later stages prior to prehaustorium formation and associates with a decrease in *PLT1* expression. We also demonstrated that at this stage, the auxin transporters PIN1/PIN2 do not have asymmetric PIN polarity but show a basal epidermal localization. Furthermore, we observed a decrease in auxin levels and an increase in cytokinin. Based on the root structure layout of *S. hermonthica* and the observed basal PIN polarity, we constructed a mathematical model that depicted the auxin distribution pattern in *S. hermonthica* roots. The model recapitulated the expected decrease in auxin levels at the elongated stage resulting from basal PIN polarity, followed by auxin depletion prior to the prehaustorium stage. Consistent with these predictions, auxin response increased in the Arabidopsis cortex when cells were in contact with *S. hermonthica*. Furthermore, blocking polar auxin transport using Naphthylphthalamic acid (NPA) inhibits prehaustorium formation supporting our model.

Our results establish a mechanistic model that explains the root developmental switch from having an active meristem toward differentiation to form the prehaustorium to invade the host plants.

Results

Cellular organization of the Striga root meristem

After germination, the Striga radicle contains a meristem that has a simple and organized structure (Raghavan and Okonkwo, 1982; Hood et al., 1998). As growth progresses, Striga roots undergo anatomical changes that lead to the formation of a prehaustorium prior to host attachment (Joel and Gressel, 2013; Yoshida et al., 2016). To understand the developmental program of Striga embryonic roots, we induced seed germination using GR24, a synthetic analog of strigolactones that stimulates Striga germination, and we performed an initial analysis in the absence of the host and

HIFs. First, we categorized the developmental stages of the Striga embryonic root. We designated these stages based on the meristematic activity of the Striga root and its cellular layout and tissue organization rather than the time after germination because of the lack of synchronization during seed germination (Figure 1, A–J). The stages are as follows: a young stage, in which the root emerges from the seed coat; at this stage, the Striga radicle has a structured root meristem, similar to that of the model plant *A. thaliana* (Figure 1, B, G, and P); a pre-elongated stage, in which cells shootward of the meristem increase in length and contribute to increasing the length of the radicle (Figure 1, C and H); an elongated stage, with only a few meristematic cells and with root hairs initiating on the lateral side of the epidermis above the meristematic cells (Figure 1, D and I); and a differentiated stage without a meristem and with root hairs emerging from the tip of the radicle (Figure 1, E and J). In mature embryo and the young stage, Striga roots have a

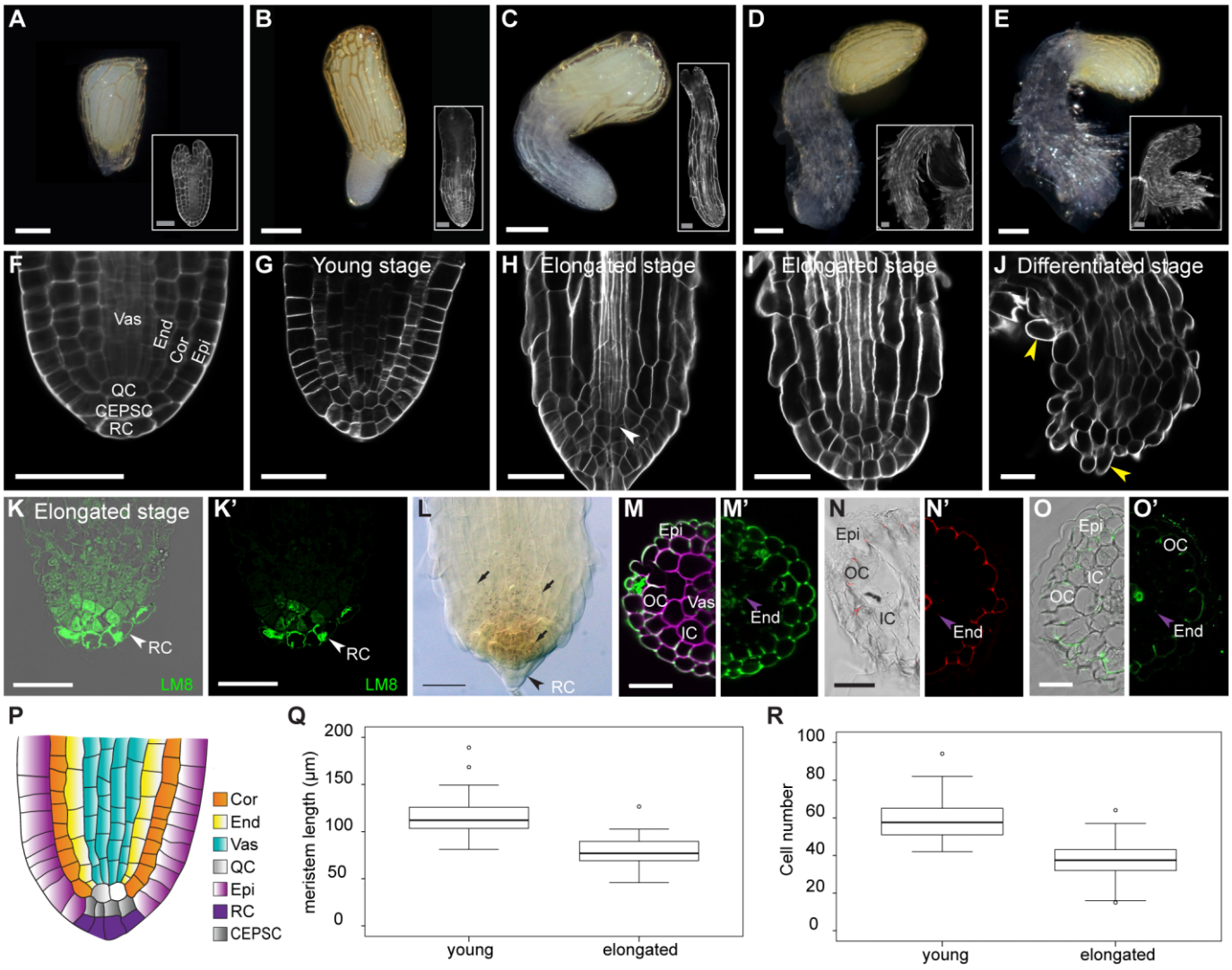

Figure 1 Cellular organization of the *S. hermonthica* root meristem. A–E, Macrophotographs of *S. hermonthica* seedlings at the following different developmental stages: A, seed; B, young; C, pre-elongated; D, elongated; and E, differentiated/prehaustorium. White rectangles show their respective confocal sections stained with Renaissance SCRI stain. F–J, Longitudinal confocal sections of the *S. hermonthica* roots stained with Renaissance SCRI stain. K–K′, Immunolocalization using the LM8 antibody to mark the root cap in *S. hermonthica*. (K a confocal overlay of transmission and fluorescence image; K′ is the fluorescent channel). L, Lugol's iodine stain showing stem cell differentiation. M–O′, Images of Striga root cross sections depicting tissue types using cell wall stains. Sections were taken from above the meristem (150–200 µm distance from the root tip). M, Renaissance stain. M′, Auto-fluorescence. N and N′, Basic fuchsine. O and O′, Berberine stain. P, Schematic representation of the *S. hermonthica* root meristem at the young stage. Times indicated in the panels are hours after GR24 treatment. Scale bars: macrophotographs in (A–E): 200 µm; Images in (A–E insets; F–O′): 50 µm. Epi, epidermis; OC, outer cortex; Exo, exodermis; IC, inner cortex, End, endodermis; Vas, vasculature; RC, root cap; Cor, cortex; QC, quiescent center (QC); CEPSC, columella and epidermal precursor cells; arrows heads pointing to root hairs (J), root cap (K–L) and casparian strips (M–O′). Q and R are boxplots for meristem size (Q) and cell number (R) in young ($N = 86$) and elongated ($N = 55$) *S. hermonthica* seedlings (24- and 48-h GR24 treatment). *N* represents the number of seedlings analyzed. Horizontal lines indicate the medians. Box limits indicate the 25th and 75th percentiles. Whiskers extend to the 5th and 95th percentiles. The circles represent outliers.

simple and organized structure with regular cell files, which is consistent with the results of previous studies (Raghavan and Okonkwo, 1982; Hood et al., 1998). From outside to inside, we could distinguish the epidermis, ground tissue (cortex and endodermis), and vasculature (Figure 1, F, G, and P). Similar to that in *A. thaliana*, we observed the quiescent center (QC)-like cells at the base of the vasculature and ground tissue layers. Following tissue lineages, we found, distal to the QC, a layer that contain cells directly in contact with the root cap and the epidermis that we named columella and epidermal precursor cells (Figure 1, F and G; Supplemental Figure S1). We also identified a single-layered root cap using the LM8 antibody, an epitope specific for xylogalacturonan that stains cells that are in the process of loosening from other tissues, such as those located at the root tip (Willats et al., 2004; Figure 1, K and K′). In Arabidopsis and other species, the distal columella comprises the columella stem cells and differentiated columella layers, of which only the differentiated columella layers accumulate starch granules (Van den berg et al., 1997). However, in *S. hermonthica*, we found starch granules in the distal root cells and the meristem, as evidenced using Lugol's iodine and pseudo-Schiff propidium iodide staining (mPSI-PI) staining (Figure 1L, Figure 2, A″–E″; Supplemental Figure S1). In addition, unlike in other plant species in which root cap cells detach and are continuously replenished during root growth (Kumpf and Nowack, 2015), we detected neither additional root cap cell layers nor root cap cell sloughing in *S. hermonthica* during root growth (Supplemental Figure S1; Figure 2, A–D).

During root growth, we observed multiplanar divisions in the meristem at the pre-elongated and elongated stages. These divisions were anticlinal in the epidermis and at cells at the QC position (Supplemental Figure S1); and periclinal in the cortex and endodermis; the latter generated additional cell files (Supplemental Figure S1). In roots, some tissue types can be defined by the composition of their cell wall (Ursache et al., 2018); therefore, we used different dyes to assess differences in cell wall composition in cross-sections of *S. hermonthica* roots. Using auto-fluorescence to detect the presence of lignin and suberin, we detected a bright fluorescent signal in the epidermis and adjacent layer, endodermis, and in a subset of vascular cells, suggesting the accumulation of lignin and suberin in these tissues (Figure 1, M and M′). The accumulation of fluorescent signal in the layer adjacent the epidermis indicates that Striga has an exodermis. These observations were confirmed using basic fuchsin and berberine fluorescent stains to monitor lignin and suberin deposition, respectively (Figure 1, N and O′).

Meristem differentiation in *S. hermonthica*

To evaluate the growth dynamics at the different developmental stages, we first measured the size of the meristem and determined the number of cells in the young and elongated stages. We found that in the elongated stage, the meristem size was reduced and contained less cells compared with the young stage (Figure 1, Q and R).

Next, we quantified the cell division rate during the different stages and in different tissue types using ethyl deoxyuridine (EdU), which is incorporated into cellular DNA during replication, marking cells in the S phase (Cruz-Ramírez et al., 2013, Figure 2, A–E″). We observed high meristematic cell division rates during the young stage (Figure 2, A, A′, and F; Supplemental Figure S2). At the pre-elongated and elongated stages, cells continued to divide at the distal meristem, including QC and columella stem cells (Figure 2, B, C′, and F). However, prior to differentiation, we observed a rapid decrease in the cell division rate in the distal root apex (Figure 2, D and F), followed by an arrest in meristematic activity (Figure 2, E–F; Supplemental Figure S2). To verify these observations, we performed RNA in situ hybridization using *HISTONE H4*, which is expressed during the progression of the G1–S phase of the cell cycle (Gutierrez, 2009; Figure 2, G and G′), and the mitotic-specific G2–M phase *CYCLIN-B1-3* (Bulankova et al., 2013; Figure 2, H and H′). Both genes were isolated from Striga based on their homology with their orthologs in Arabidopsis. We found that the expression levels of both *ShHISTONE H4* and *ShCYCLIN-B1-3* decreased as the meristem underwent differentiation (Figure 2, G–H′).

In Arabidopsis, the loss of activity of *PLT* leads to the loss of stem cell activity, the reduction of cell division rates, and differentiation of root meristem (Aida et al., 2004; Galinha et al., 2007). Therefore, we used *PLT* to evaluate whether progression to prehaustorium formation was associated with the loss of stem cell activity. RNA in situ hybridization using a probe of the Striga homolog of Arabidopsis *PLT1 and PLT2* (*ShPLT1/2*, Supplemental Figure S3) revealed high mRNA levels in the meristem, and these levels decreased during prehaustorium formation (Figure 2, I and I′).

Prehaustorium induction can occur in the absence of HIFs but less efficiently

Striga prehaustorium can grow in the absence of HIFs (Supplemental Figure S4 and Supplemental Tables S1 and Table S2; Cui et al., 2018), however, it has been established that prehaustorium formation is triggered by host-derived HIFs (Cui et al., 2018), we then sought to compare the growth and tissue anatomy of Striga roots grown with and without HIF. To this aim, we used the well described and commercially available DMBQ (Chang et al., 1986; Wada et al., 2019) and rice (*Oryza sativa*) extracts, containing host-derived HIF (Cui et al., 2018; Wada et al., 2019). We also used root extract from Arabidopsis, as it has been shown to induce haustorium formation in Striga despite not being a host (Cui et al., 2018). As a control we used half-strength Murashige and Skoog (MS) medium without extracts. In all treatments, Striga was able to develop a prehaustorium (Supplemental Figures S4 and S5). However, the rate of prehaustoria formation was higher in plants treated with extracts obtained from rice (92%) or with DMBQ (93%) compared with Arabidopsis extract (59%) or control (10%, Supplemental Table S1 and Supplemental Figure S5). Next, we assessed meristem activity in the presence and absence

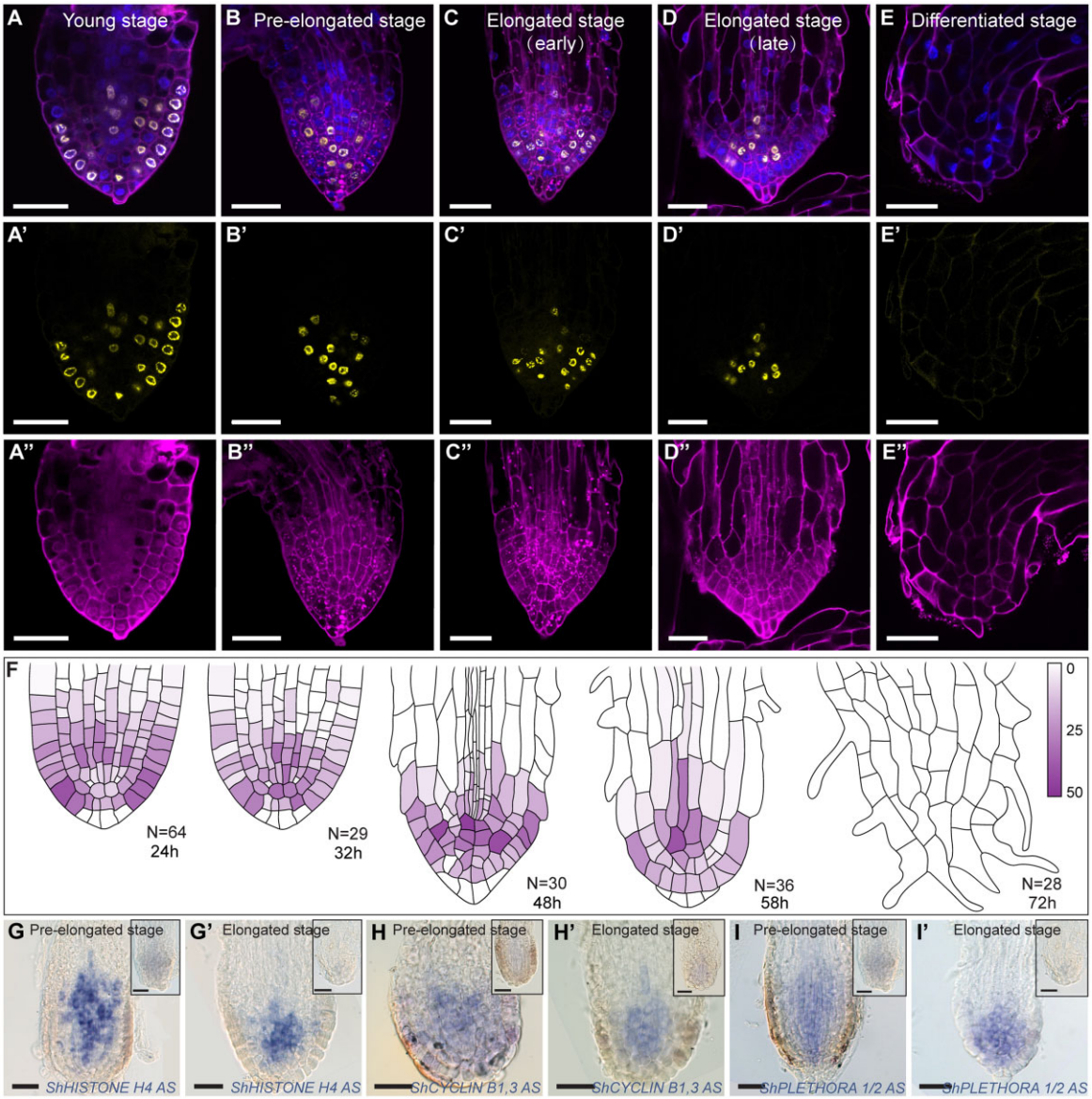

Figure 2 Prehaustorium formation associates with meristem differentiation. A–E″, Confocal images of *S. hermonthica* roots stained with the cell wall stain mPS-PI (A″–E″, purple), EdU (A′–E′; yellow), and the nuclear stain Hoechst (blue in A–E). A–A″, young stage; B–B″, pre-elongated stage, C–C″, early elongated stage, D–D″, late elongated stage; E–E″, differentiated stage, F, quantification of the cell division rate during root differentiation. Colored bar indicates the percentage of cell division. RNA in situ hybridization during meristem differentiation in longitudinal sections using *ShHistone-H4* (G–G′), *ShCYCLIN B1,3* (H–H′), and *ShPLETHORA1/2* (I–I′) probes. Roots in the upper right of the images represent the sense control for each probe. *Striga hermonthica* seedlings with 24- or 48-h GR24 treatment. All scale bars: 50 μm.

of HIF using EdU staining. We found that roots treated with HIF also showed a reduced meristematic activity similar to water treatment (Figure 3, A–G; Supplemental Figure S5). We also checked whether HIF can affect the expression of the meristematic gene *ShPLT1/2* and found that *ShPLT1/2* expression also decreases at the prehaustoria stage similar to when grown in absence of HIF (Figure 3, H–I″).

Prehaustorium formation is associated with changes in auxin and cytokinin levels

Because *PLT* expression is regulated by auxin (Aida et al., 2004; Mähönen et al., 2014), the decrease in *PLT1* levels in Striga roots during the transition to the prehaustorium stage prompted us to investigate whether an alteration in the auxin distribution pattern also contributes to meristem differentiation. In the Arabidopsis meristem, auxin maxima define cell-type organization and dictate root zonation during root growth (Sabatini et al., 1999; Grieneisen et al., 2007; Dello Ioio et al., 2008). Furthermore, root zonation is modulated by the antagonistic effect of auxins and cytokinins, with high levels of cytokinins promoting elongation and differentiation and high auxin levels inducing cell division (Moubayidin et al., 2010). Therefore, we sought to visualize auxin and cytokinin distribution during Striga prehaustorium

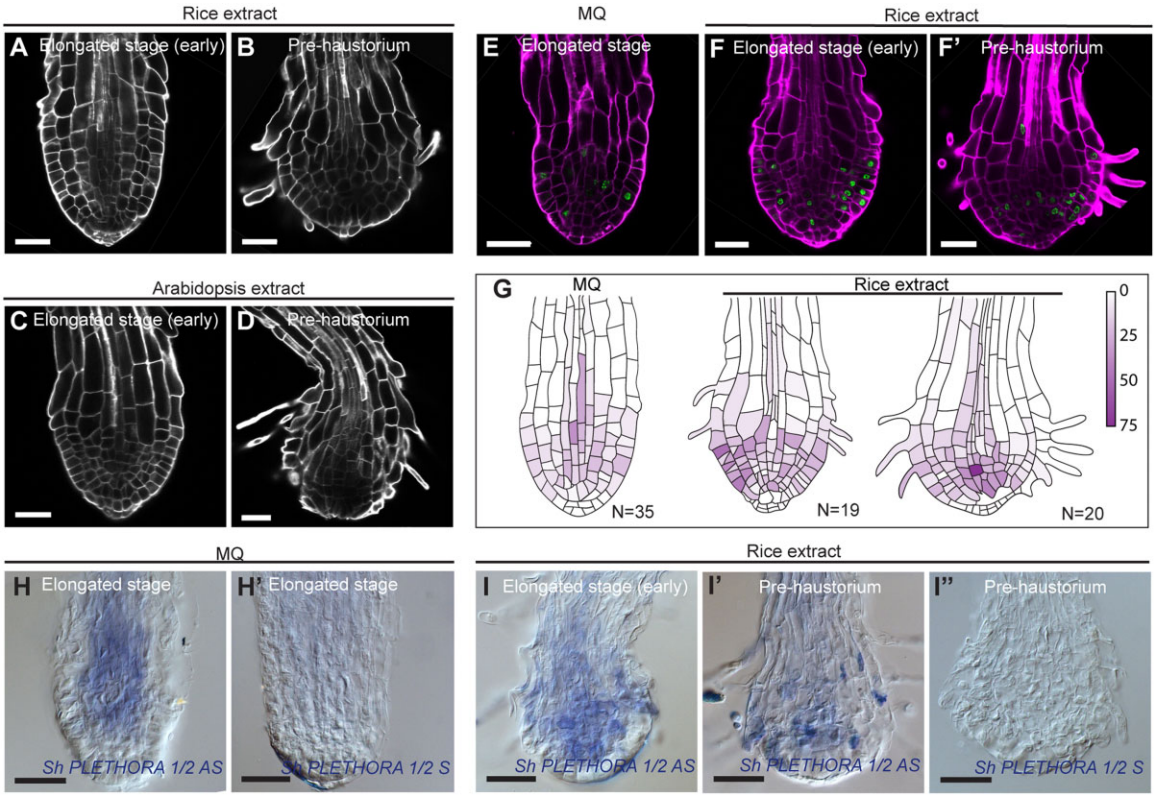

Figure 3 Prehaustorium of *S. hermonthica* induced by host and nonhost root extract treatment. A–D, confocal images of Striga roots treated with rice (A and B) and Arabidopsis (C and D) roots extract. Roots were stained using Renaissance SCRI stain. Roots were treated after 24 h of germination in presence of GR24 and imaged after 4 and 12 h after treatment with root extracts. E and F′, EdU staining showing cell division in the differentiating *S. hermonthica* roots. G, quantification of the cell division rate during prehaustorium formation. Colored bar indicates the percentage of cell division. H–I″, RNA in situ hybridization during prehaustorium formation in longitudinal sections using *ShPLETHORA1/2*. H–H′ are roots germinated in MQ water. I–I″ roots treated with rice extract for 12 h after 24 h of germination. MQ, Milli-Q water, AS, Antisense, S, sense control. All scale bars: 50 µm.

formation using anti-indole-3-acetic acid (IAA) and anti-cytokinin antibodies (Mravec et al., 2017; Agrisera, AS09 437) by immunolocalization in paraffin-embedded sections of *S. hermonthica* roots grown in water or with rice exudates (Figure 4, A–D′). In both water and rice exudates, the anti-IAA antibodies showed a high signal at the pre-elongated stage (Figure 4, A and A′). This signal became restricted to only a few cells at the root tips prior to root differentiation (Figure 4, B, B′, D, and D′).

The anti-cytokinin antibodies exhibited an antagonistic pattern to auxins (Figure 4, E–H′). More cells at the pre-haustoria stages displayed the anti-cytokinin signal, while only a few cells were detected by the anti-IAA antibodies (Figure 4, D and H).

Auxin has been shown to stimulate root growth and delay root differentiation (Dastidar et al., 2019). Hence, we investigated whether the application of auxin prevents Striga meristem differentiation and delays prehaustorium formation. Because we did not observe striking differences between *S. hermonthica* roots grown in water and those grown in HIF and to assess the specificity of auxin, we used *S. hermonthica* grown in water. We incubated young *S. hermonthica* (48 h after induction with GR24) with different IAA concentrations and monitored root growth and cell division rates within the meristem using EdU (Figure 4, I–K; Supplemental Figure S6). Three days after germination (dag), only 18% of untreated *S. hermonthica* showed active division in the meristem. This proportion was much higher following the application of IAA concentrations for one day and was approximately 40% at 10^{-8}, 42% at 10^{-7}, and 32% at 10^{-6} M IAA. After treatment for 2 days (4 dag), only 6% of the control seedlings retained an active meristem, whereas treated *S. hermonthica* maintained their meristem with 39% at 10^{-8}, 44% at 10^{-7}, and 29% at 10^{-6} M IAA. At day 3 after auxin application (5 dag), we observed 17% at 10^{-8}, 6% at 10^{-7}, and 15% at 10^{-6} M IAA. IAA at a higher concentration, i.e. 10^{-5} M, inhibited cell division and elongation (Supplemental Figure S6). As *S. hermonthica* exhibited the highest rate of cell division on day 2 and at 10^{-8} and 10^{-7} M IAA, we focused on this time point and monitored cell division rates using 10^{-8} and 10^{-7} M IAA, which confirmed that auxin delayed *S. hermonthica* root differentiation (Figure 4K). Next, we tested whether a decrease of auxin levels promoted prehaustoria formation. The auxin biosynthesis inhibitor L-kynurenine (He et al., 2011) increased the rate of prehaustoria (30%) compared to when plant where treated only with water (10%; Supplemental Table S1 and Supplemental Figure S5).

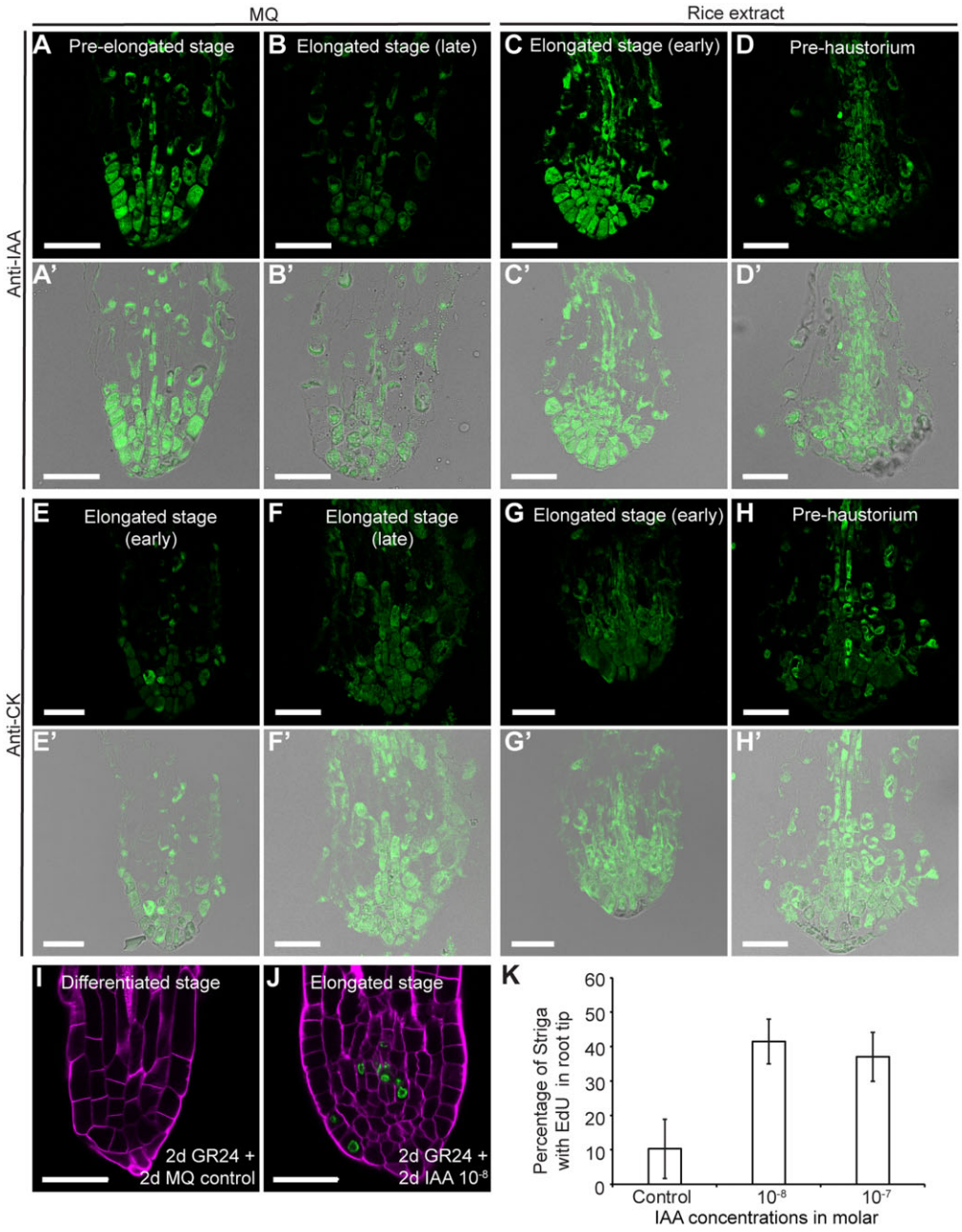

Figure 4 Auxin–cytokinin homeostasis control of *S. hermonthica* meristem activity. A–D′, immunolocalization showing auxin distribution in *S. hermonthica* root sections using anti-IAA antibody, $N = 30$; E–H′, cytokinin accumulation using anti-cytokinin antibody. Seedlings are 24 (A and E) and 48 h (B and F) after GR24 treatment-induced germination and 12 h (C, G, D, and H) of rice extract treatment. $N = 20$; A–D and E–H are fluorescence channel; A′–D′ and E′–H′ are overlay fluorescence and transmission light channels. I–K, IAA application delayed meristem differentiation in the *S. hermonthica* radicle, as monitored by EdU staining. I and J, Confocal images of control (I) and IAA-treated roots (J). MQ, Milli-Q water. K, Percentage of root containing cells undergoing cell division (EdU-stained cells) in *S. hermonthica* roots treated with different molar IAA concentrations. Columns indicate the means generated from three biological replicates; error bars represent SE. A significant difference from the value of the non-treated roots versus IAA-treated roots was determined by *t* test ($P < 0.05$). The number of *S. hermonthica* seedlings used were as follows for the control ($N = 44, 53, 40$); 10^{-8} ($N = 43, 45, 48$); 10^{-7} ($N = 93, 107, 95$). *N* represents the number of seedlings used from three independent biological replicates. All scale bars: 50 μm.

A basal PIN polarity precedes prehaustorium formation

In Arabidopsis, the PIN proteins, which serve as auxin efflux facilitators, play a major role in controlling the root meristem size by maintaining auxin maxima through establishing an auxin reflux loop in the meristem (Blilou et al., 2005). Furthermore, tissue-specific PIN polarity at the plasma membrane acts as a determinant for auxin flow directionality (Wisniewska et al., 2006). To determine whether the loss of meristematic activity during prehaustorium formation in

Striga roots is also modulated by changes in PIN expression we monitored the expression of PIN mRNA by in situ hybridization using Striga *PIN1* and *PIN2* genes.

We identified Striga PIN homologs using the recently published *Striga asiatica* genome sequence (Yoshida et al., 2019; Supplemental Figure S7). RNA *in situ* hybridization showed that unlike Arabidopsis, the Striga *PIN1* ortholog is not restricted to the vasculature but its expression extends to all tissues including the epidermis (Figure 5, A and A′). Next, we monitored PIN2 expression, and, unlike Arabidopsis *PIN2*, which is usually expressed in the cortex and epidermis, we also detected *ShPIN2* in the vasculature (Figure 5, B and B′).

Next, we evaluated PIN polarity using Arabidopsis-derived PIN1 (Gälweiler et al., 1998) and PIN2 antibodies (Müller et al., 1998) in *S. hermonthica* roots. Both PIN1 and PIN2 antibodies have been shown to recognize PIN orthologues in other plants species and can thus be used as tools to evaluate auxin flux within the root meristem (Lee et al., 2009; Ivanchenko et al., 2015; Pasternak et al., 2015).

In the Arabidopsis root meristem, PIN1 is localized at the basal end of the vasculature cells (Gälweiler et al., 1998). PIN2 is expressed in the cortex and epidermis and localizes at the apical side of cells in the epidermis and basally in the cortex (Blilou et al., 2005). In Striga roots, we did not detect signal using the Arabidopsis PIN1 antibody in the vasculature but rather in the epidermis with lateral and basal polarity at the early stage (Figure 5, C and C′). At the elongated stage, PIN1 was predominantly located basally at the epidermal layer within the root tip (Figure 5, D and D′). The PIN2 antibody on the other hand detected apical and basal polarity in the epidermis at the early stage (Figure 5, E and E′; Supplemental Figure S8). At the elongated stage, PIN2 was located basally and laterally outward from the epidermis and the cells located at the columella position (Figure 5, F and F′; Supplemental Figure S8).

The observed basal PIN localization indicates that auxin is transported out of Striga root. To test whether auxin transport is important for prehaustoria formation, we treated Striga seedlings with the polar auxin transport inhibitor NPA and monitored the rate of prehaustoria formation (Supplemental Figure S5). We found that NPA reduced the rate of prehaustoria formation with and without rice extracts (Supplemental Figure S5 and Supplemental Table S2). In addition, when treated with NPA, auxin became evenly distributed throughout the meristem (Supplemental Figure S5). The reduction of prehaustoria formation in the presence of auxin transport inhibitors is consistent with previous reports (Tomilov et al., 2005).

Taken together, our data highlight the importance of PIN polarity and auxin transport in the process of prehaustoria formation.

A decrease of auxin in Striga roots mediates prehaustorium formation

At the elongated stage, PINs displayed a basal polarity in cells located at the root cap position (Figure 5). To predict the dynamics of auxin distribution in the Striga root during growth, we adapted an established mathematical model for Arabidopsis roots (Savina and Mironova, 2020) based on Striga root developmental layouts (Figures 1 and 2) and PIN1 and PIN2 expression patterns and polarity (Figure 5). The model considers mutual interactions between auxin and PIN dynamics issued from positive and negative self-regulations of auxin transport (Supplemental Methods S1; Figure 5). We implemented the principle difference between Striga and Arabidopsis models in which PINs were able to localize on the outer membranes at the root cap position. With these localization patterns and in the absence of auxin reflux, we anticipated that auxin would be excreted from the roots to the environment.

Accordingly, we developed three 2D cell layouts mimicking longitudinal root sections at the early young, elongated, and pre-elongated stages (Supplemental Figures S1 and S9). The model parameters were adjusted to obtain auxin distribution, with an Arabidopsis-like auxin pattern having the maximum at the QC and high auxin levels in the root cap (Figure 6, A, D, and G; Supplemental Figure S10, A–D). This was obtained when the negative regulation of PIN1/2 expression at high auxin levels and positive regulation at low levels were considered. Next, we entered the generated pattern at the young stage for PINs and auxin into the cell layout to the pre-elongated stage where cells elongated but without an increase in the cell division rate (Supplemental Figure S9) and continued the calculations without changing the model parameters or equations. As a result of auxin dilution caused by cell elongation, we observed both a decrease in the auxin maximum (Figure 6B; Supplemental Figure S10) and a shift in PIN localization domains toward the root cap (Figure 6, E and H). The auxin levels in the QC were reduced compared to those observed for the proximal meristem at the early stage, in which active cell division occurs (Figure 6, J and K). The reduction in auxin levels promotes cell division. Moreover, with high PIN1 expression in cells at the root cap position (Figure 6M), Striga begins excreting auxin into the environment and depleting auxin from the root tip (Figure 6L). Interestingly, we observed a robust analogy for the PIN1 and PIN2 expression domains between the simulation (Figure 6, D–I; Supplemental Figures S9 and S10) and experimental results (Figure 5; Supplemental Figure S8). When the calculations were implemented for the elongated stage layout, we found high PIN1 and PIN2 expression in the cells located at the root cap position where auxin was excreted more efficiently from the *S. hermonthica* roots (Figure 6; Supplemental Figure S9).

Our model indicates that Striga excretes auxin during root differentiation/prehaustorium formation. Because Arabidopsis root exudates could also induce prehaustorium formation (Figure 3, D–F; Supplemental Figure S5), we used the Arabidopsis auxin response reporter lines *DR5::vYFP* (high auxin response) and *DII::VENUS* (low auxin response) to evaluate whether Striga induces changes in auxin levels or distribution when in contact with Arabidopsis roots (Figure 6, R

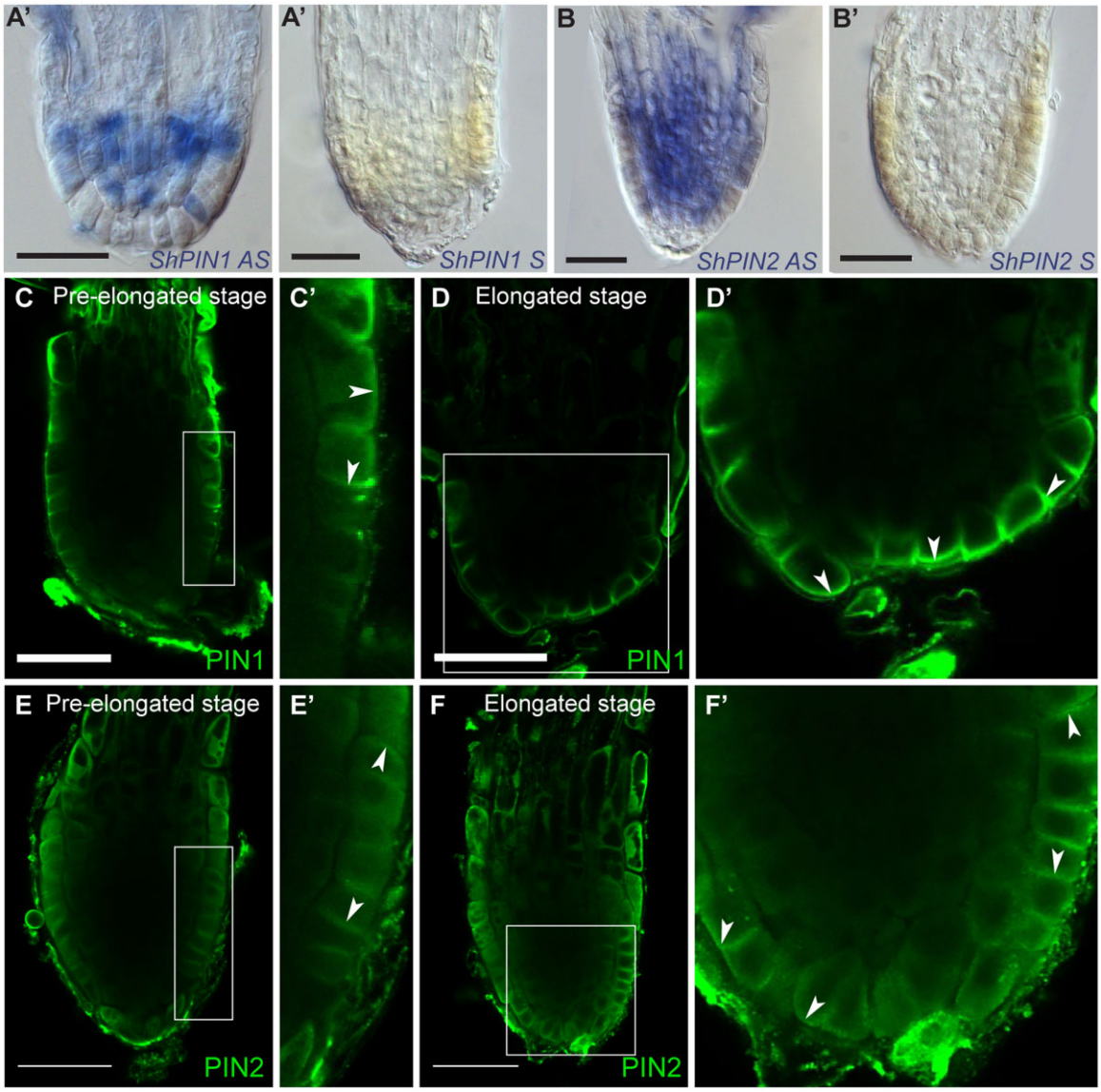

Figure 5 PIN protein expression and polarity in *S. hermonthica* during root differentiation. A–B′, RNA in situ hybridization of *S. hermonthica* root meristems in longitudinal sections using *ShPIN1* (A–A′) and *ShPIN2* (B–B′). A and B are the antisense probes and A′ and B′ are the sense control probes. C–F′, Immunolocalization using *Arabidopsis thaliana* PIN1 and PIN2 antibodies showing (C–D′) basal PIN1 in the epidermis. C′ and D′ are insets from C and D, respectively. *N* = 30. E and F′, PIN2 localization showing epidermal apical, lateral, and basal polarity. Arrows indicate the shift in PIN polarity. E′ and F′ are insets from E and F, respectively. *Striga hermonthica* seedlings were treated with GR24 for 24 or 48 h. *N* = 60. All scale bars: 50 μm.

and S). Using time-lapse imaging, we evaluated and quantified the fluorescence levels in both the epidermis and cortex of *A. thaliana* roots in contact with *S. hermonthica* from the young stage to the formation of prehaustoria (Figure 6, O–Q′). We observed ectopic accumulation of *DR5::vYFP* fluorescence and reduction of the *DII::VENUS* fluorescence signal in the root epidermis and cortex when the prehaustorium began to be formed and was physically attached to the Arabidopsis root (Figure 6, R and S; Supplemental Movie S1). No expression in the cortex was observed when the *S. hermonthica* root did not differentiate or when it failed to reach the Arabidopsis root (Supplemental Figure S11 and Supplemental Movies S2 and S3). These results are in agreement with those of our model and support the idea that auxin is depleted from the meristem prior to prehaustorium formation.

Discussion

Root parasitic weeds undergo developmental programming to form their invasive organ, termed the prehaustorium, which emerges from the roots (Joel, 2013). The prehaustorium is essential for penetrating the host and deploys haustorial hairs by combining mechanical pressure and excreted cell wall-degrading enzymes (Reiss and Bailey, 1998; Perez-de-Luque, 2013). The germination of parasitic plants and the formation of prehaustoria are the most studied events in

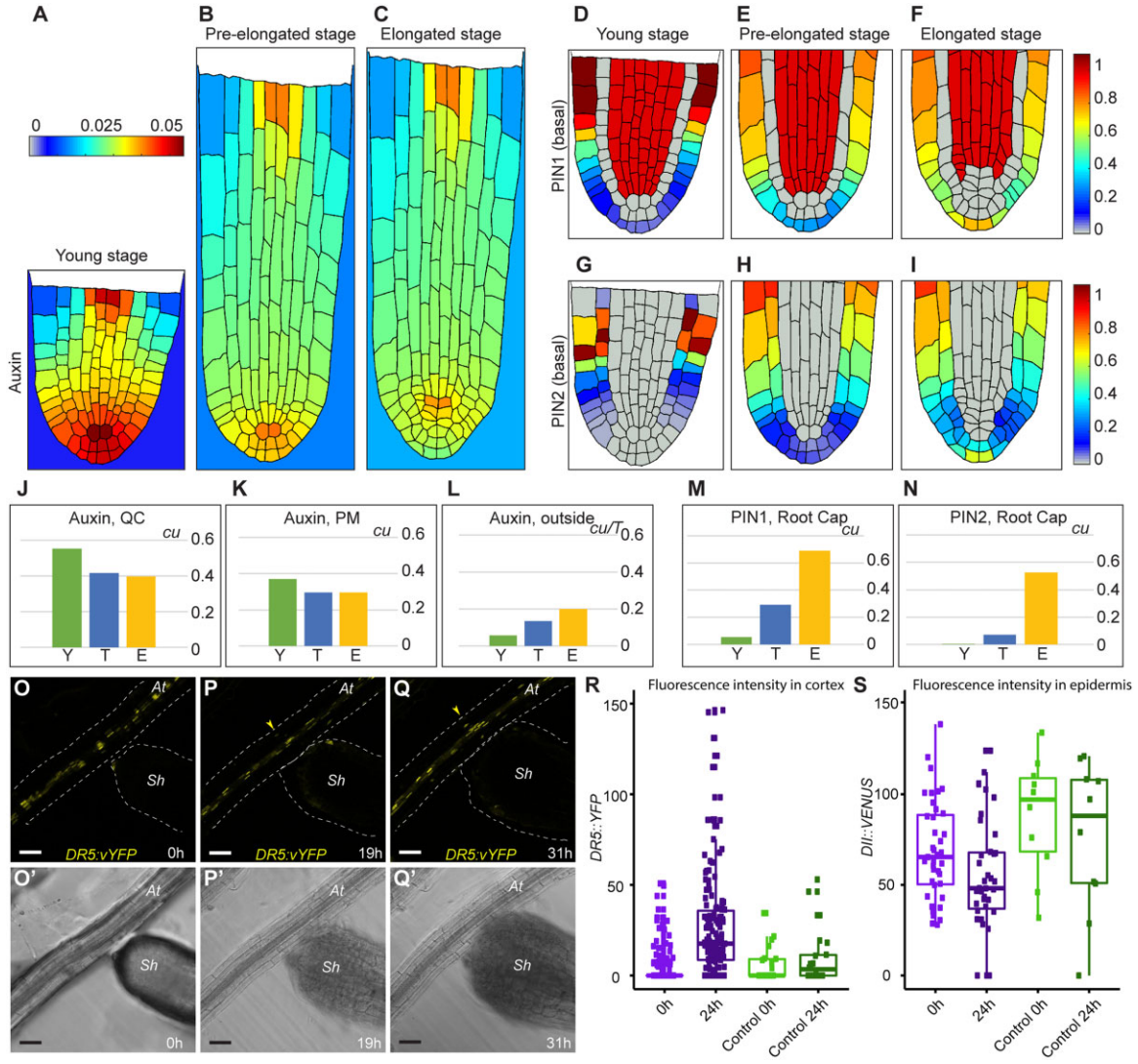

Figure 6 Mathematical model depicting auxin distribution in *S. hermonthica* during root growth. (A–C), Quasi-steady state in auxin distribution inside and outside the *Striga* root at three consequent developmental layouts. (A, D, and G) Young stage (Y), (B, E, and H) pre-elongated stage (T), and (C, F, and I) elongated stage (E). D–F, PIN1 localization, G–I, PIN2 localization with basal polarity. PIN2 with apical polarity is depicted in Supplemental Figure S9. The color scale bars are concentration units (cu). J–N, Comparison of the variable values between the stages. Auxin levels in the QC (J); in the proximal meristem (PM) (K); excreted from *S. hermonthica* roots (L) during calculation time *T*. M, PIN1 levels in the root cap; N, the level of basally polarized PIN2 in the root cap. cu, concentration units. O–Q′, time-lapse images of germinating *S. hermonthica* in contact with Arabidopsis roots containing *DR5::vYFP*. *S. hermonthica* were used 24 h after germination, $N = 10$. O–Q, Fluorescence YFP channel. O′–Q′ PMT transmission channel. Arrowheads indicate ectopic *DR5::vYFP* expression in P, Q at *A. thaliana* (*At*). *sh*, *S. hermonthica*. Scale bars: 50 µm. R, the DR5 fluorescence values are significantly increased after 24 h when the Striga root differentiates in contact with Arabidopsis roots (two-tailed *t* test, $P = 0.03794$). The DR5 values are not significantly different when physical contact is not established with the Arabidopsis roots (two-tailed *t* test, $P = 0.4947$). S, the DII fluorescence values are significantly decreased after 24 h when the Striga root differentiates in contact with Arabidopsis roots (two-tailed *t* test, $P < 2.2e{-}16$) the DII fluorescence are not significantly different when physical contact is not established (two-tailed *t* test, $P = 0.3095$). Control are striga plants that have not been in contact with Arabidopsis. Box limits indicate the 25th and 75th percentiles. Whiskers extend to the 5th and 95th percentiles. Points indicates the data.

these invasive species because they form a putative point of attack to the invasion of crop plants (Okonkwo and Raghavan, 1982; Baird and Riopel, 1983; Kountche et al., 2016). Many studies have focused on either the transcriptional response (Ranjan et al., 2014; Yang et al., 2015; Yoshida et al., 2019) or the developmental characteristics of lateral haustoria (Ishida et al., 2016; Wakatake et al., 2020), which develop through de-differentiation from mature cells in the cortex, resembling lateral root emergence or nodule formation during symbiosis with rhizobia (Yoshida et al., 2016).

In this study, we assessed the developmental programs governing the formation of prehaustoria in *S. hermonthica*, the structure that will develop into the terminal invading haustorium. In many root parasitic plants, including the holoparasitic Orobanche and other Striga species, the

development of terminal prehaustoria is essential for penetrating the host roots. As these parasitic plants have small seeds and thus constrained nutrient availability, their survival relies entirely on developing a terminal prehaustorium to invade the host shortly after germination and exploits and hijacks its nutrient supply. Our results highlight how developmental programs governs the shift from a conventional root meristem to an invasive organ.

Our tissue anatomy analysis, consistent with those of a previous study (Hood et al., 1998), revealed that *S. hermonthica* embryonic roots, regardless of whether they are grown with or without HIF, have a meristem organization similar to that of *A. thaliana* (Figure 1). Although we detected a root cap in *S. hermonthica* roots (Hood et al., 1998), we did not observe root cap sloughing during root growth, unlike in other plant species (Supplemental Figure S1). In nonparasitic plants, the release of outer root cap cells into the soil decreases the frictional resistance (Bengough and McKenzie, 1997). However, in Striga, this function might be required only for a short period of growth until reaching the host's roots.

During the young stage, *S. hermonthica* roots possessed a meristem with active cell division, which is in accordance with the results of a previous study on *P. japonicum* roots (Ishida et al., 2016). During progression to the prehaustorium stage, we observed increased cell division in the stem cell niche area, including QC cells (Figure 2). This is in contrast to the observations in Arabidopsis, in which QC cells undergo infrequent cell division. The observed increase in QC cell divisions might be a consequence of the accumulation of cytokinins in the distal meristem, as suggested previously (Zhang et al., 2013, Figure 3). Alternatively, these divisions might result from the induction of stress signaling pathways. In Arabidopsis, elevated levels of the defense hormone jasmonic acid (JA) induce QC cell division (Zhou et al., 2019). Therefore, it is plausible that JA signaling contributes to the observed division in the *S. hermonthica* stem cell niche area, as supported by the enrichment in genes involved in response to wounding during haustorium formation (Ishida et al., 2016). The levels of reactive oxygen species (ROS) also play a role in modulating QC cell division (Lee, 2019; Yamada et al., 2020). Recent studies have reported an increase in peroxidase (precursor of ROS) activity during terminal and lateral haustoria formation (Wada et al., 2019; Yoshida et al., 2019). In most plants, the QC serves as a reservoir to replenish root stem cells during their growth. However, in Striga, QC signaling occurs transiently and might be required only for the establishment of the meristem at the young stage.

Although the progression to meristem differentiation in *S. hermonthica* roots was similar when the plants were grown in water or treated with HIFs, the cellular layout of the roots differed between these two conditions. When grown in water, *S. hermonthica* roots maintained their regular structure and displayed organized division planes (Figure 1). When treated with HIFs, the cells divided in an unorganized manner (Figure 3), which might have resulted from microtubule disorganization, as described during prehaustorium formation in the parasitic plant Cuscuta (Kaštier et al., 2018). With the complex composition of HIFs obtained from root exudates, many components have been shown to affect cell division, including terpenoids and flavonoids (Albrecht et al., 1999; Woo et al., 2005; Chaimovitsh et al., 2012). Upon progression to prehaustorium formation, we observed a reduction in the rate of cell division, followed by meristem differentiation (Figures 2 and 3). Our results corroborate those of transcriptomic studies showing downregulation of DNA metabolism genes during haustorium formation (Torres et al., 2005).

Our findings also revealed the importance of hormone homeostasis for prehaustorium formation (Figure 4). In Arabidopsis, a balance between auxins and cytokinins dictates root zonation and an increase in cytokinin levels mediates meristem differentiation (Moubayidin et al., 2010). Additionally, the establishment of an auxin maximum through polar auxin transport dictates cell fate, cell division planes and rate, and cell polarity (Sabatini et al., 1999; Blilou et al., 2005). We showed that in *S. hermonthica* roots, differentiation at the stem cell region is associated with a decrease in auxin levels at the root tip and an increase in cytokinin levels prior to prehaustorium formation (Figure 4, A–H′).

We also demonstrated that the decrease in auxin levels at the root tip is coincided with a shift in PIN polarity (Figure 5). In Arabidopsis, polar distribution of PIN proteins in the plasma membrane in a tissue-specific manner directs the auxin flux required for establishing the auxin maximum in the root meristem. In *S. hermonthica*, we found that the PIN auxin efflux carrier detected by the Arabidopsis PIN2 antibody is not localized at the apical site of the epidermis but rather at the basal site of the cell. In addition, the PIN transporter detected by the PIN1 antibody has distinct tissue localization compared with that in Arabidopsis. It is important to note that these antibodies are valuable tools to predict the auxin routes in the meristem but cannot be used to extrapolate or predict specific plant species cell type localization. The tissue-type Striga PIN protein polarity can only be established using Striga PIN proteins. However, such analysis will only be possible when a stable transformation protocol is available in Striga. The differences in PIN localization suggest that *S. hermonthica* might use different polarity determinants in the epidermis.

Our results are consistent with those of recent studies regarding the localization of PjPIN1 and PjPIN2 in *P. japonicum* during early haustorium formation (Wakatake et al., 2020). Both PjPIN1 and PjPIN2 accumulated at the basal end of cells toward the host cells (Wakatake et al., 2020). Since the PIN protein localization has been shown to predict auxin transport routes (Blilou et al., 2005), the orientation of PINs at the outer side of the cells in Striga roots indicates that auxin is transported away from the meristem and suggests a reduced basipetal-shootward auxin transport which

leads to a decrease of auxin level and subsequently a loss of the meristem in *S. hermonthica* (Figures 5 and 6). NPA treatment of Striga roots delayed prehaustorium formation. Since blocking auxin transport using NPA alters auxin distribution in the roots through inhibiting the PIN proteins (Sabatini et al., 1999; Abas et al., 2021), the observed delay in prehaustorium formation in Striga is possibly due to the impaired PIN function leading to inefficient auxin excretion from the root tip. The redistribution of auxin throughout the Striga meristem in plant treated with NPA is in agreement with these observations (Supplemental Figure S5).

Furthermore, blocking auxin biosynthesis in Striga roots using the auxin competitor L-Kynurenine increased the rate of meristem differentiation, confirming that auxin reduction during Striga root growth is essential for prehaustoria formation.

A study using a mesoscopic model in Arabidopsis established that a robust auxin maximum is generated by combining root topology, PIN protein distribution, and membrane permeability (Grieneisen et al., 2007). The concentration of PIN proteins depends largely on auxins, with PIN1 and PIN2 expression activated at a low auxin concentrations (Vieten et al., 2005). Our results using IAA antibodies indicated low auxin levels and high PIN1 and PIN2 levels at the epidermis. Our 2D mathematical model recapitulated the decrease in auxin levels (Figure 6B; Supplemental Figure S10) and a shift in PIN proteins toward the outer layers (Figure 6, D and I). Most importantly, with a decrease in auxin levels, the concentration of PIN1 increased in the outer layers, leading to auxin depletion in the root tip and meristem differentiation. Consistent with the decrease in auxin levels, exogenous IAA application delayed prehaustorium formation (Figure 4) while reducing auxin levels by blocking its biosynthesis increased the rate of prehaustoria formation. These results are in agreement with those of a previous study, in which exogenous auxin application poised the transition to the haustorium stage and cytokinin treatment induced haustorium formation (Keyes et al., 2001). While our data indicate that a decrease in auxin concentration is required for meristem differentiation, a process that precedes prehaustoria formation, other studies showed that the establishment of the haustoria within the host correspond to an increase in auxin biosynthesis (Ishida et al., 2016). These differences can be explained either by a change in auxin levels in Striga roots after prehaustoria formation. Alternatively, the process of terminal prehaustoria formation might involve different auxin dynamics than the lateral prehaustoria which forms from the de-differentiation of the vasculature and cortex cells. Collectively, these results highlight the importance of auxin distribution mediated by asymmetric PIN protein localization not only in Arabidopsis but also in Striga. The control of auxin flow and maintenance of the auxin maxima in the root meristem remains a conserved mechanism for directing tissue patterning and sustaining root growth.

Auxin excretion from Striga roots not only leads to Striga meristem differentiation and triggers prehaustorium formation but may also contribute to host invasion. In Arabidopsis, auxin promote cell wall loosening by creating an acidic environment that stimulates cell wall remodeling enzymes (Majda and Robert, 2018). This strategy is also used by cyst and root-knot nematodes that can manipulate auxin signaling in their host plant to facilitate infection (Kyndt et al., 2016). It is plausible that the excreted auxins lead to an increase in auxin levels in the host cortex, which might contribute to cell wall degradation by activating host-specific cell wall-loosening proteins that facilitate host root invasion.

While our results provide a mechanistic understanding of developmental processes that lead to terminal haustorium formation, transcriptome analysis during haustorium formation suggested an increase in auxin levels, indicated by the enrichment of genes involved in auxin signaling and transport, such as AUX/IAAs (Yoshida et al., 2019). We also observed an increase in cytokinin levels, which has been reported to induce haustorium formation and enhance the aggressiveness of the parasitic plant *Phelipanche ramosa* (Goyet et al., 2019).

Conclusions

With the severe Striga infestation in sub-Saharan Africa due to the large number of seeds produced by each plant and their capacity to persist in the soil for almost a decade, one promising approach for reducing Striga invasion is suicidal germination, wherein synthetic stimulants are applied to the soil to induce germination in the absence of the host (Kountche et al., 2019). Preventing meristem differentiation by application of either auxin or a metabolite with a similar effect might be an alternative approach to suicidal germination by preventing prehaustorium formation and thereby infestation by the parasite.

Materials and methods

Striga hermonthica seed germination and growth conditions

Striga hermonthica seeds were collected from sorghum (*Sorghum bicolor*) fields in Sudan. The seeds were first surface-sterilized with 50% v/v commercial bleach solution (NaOCl) in water for 12 min on a rotary shaker. The seeds were then washed six times with double-autoclaved water and placed on nylon filter paper moisturized with sterile water. Preconditioning was performed at 30°C in the dark for 10 days in sterile water. Germination was induced by application of 2.5-μM *rac*-GR24 for 24 h, either directly in water with or without filter paper or in half-strength MS growth liquid medium.

Measurement of meristem size

Meristem length was measured from the cell above the root cap to the first elongated cell within the epidermis. All box

plots were generated using IBM SPSS Statistics for Windows, version V26.

Evaluation of cell division using EdU staining

EdU was added at a final concentration of 5 μM to seeds treated with GR24 and incubated in half-strength MS plant growth medium supplemented with 1% sucrose, for 90 min (Figure 2) or 12 h (Figures 3 and 4). EdU staining was performed using the Click-iT EdU Alexa Fluor 488 Imaging Kit (C10637; Invitrogen, ThermoFisher scientific, USA) as described previously (Cruz-Ramírez et al., 2013; Kirschner et al., 2017). The samples were cleared in chloral hydrate solution for several days (Truernit et al., 2008), followed by cell wall and DNA counterstaining using mPS-PI and Hoechst solution (5 μg mL^{-1}; Invitrogen) or SCRI Renaissance staining SR2200, as described previously (Musielak et al., 2015). Images were captured using an inverted confocal microscope (Leica SP8 or LSM 880, Carl Zeiss 710). All images were captured using 40× oil immersion objectives. A 405 laser was used for SCRI Renaissance and Hoechest stains with 1% of laser intensity, 750 gain, 1 AU pinhole diameter and a detection range of 410–502. A 488 laser was used for Alexa Fluor 488 with 9% of laser intensity, 600 gain, 1 AU pinhole diameter and a detection range of 504–540. A 514 laser was used for mPS-PI with 4% of laser intensity, 590 gain, 1 AU pinhole diameter and a detection range of 527–660.

Quantification of cell division rate

The cellular tissue layouts of *S. hermonthica* roots were generated manually based on confocal images. EdU-stained images were classified into different groups based on their developmental stages. Individual PI/Hoechst/Edu-stained images from each stage were manually overlayed with the cellular layouts and the number of stained nuclei were mapped manually to their respective position within the tissue. Edu-stained nuclei in every cell at every position within the meristem were counted to generate the heatmaps. Cell division rate was calculated as follow: EdU marked nuclei/*N*100). *N* is the number of plants

Starch staining using Lugol's iodine

Seedlings were incubated with Lugol's iodine and mounted in chloral hydrate solution as described previously (Van den berg et al., 1997). Images were acquired using a transmitted light illumination Leica DM2500 microscope with an HC PL FLUOTAR 40× objective.

Staining of cell walls and nuclei

To visualize the cell wall, SCRI Renaissance staining SR2200 was used as described previously (Musielak et al., 2015). For visualization of lignin and suberin, *S. hermonthica* roots were embedded in low-melting point agar and sectioned using a vibratome as described previously (Xiao et al., 2019). Sections were taken above the meristem (150- to 200-μm distance from the root tip). The sections were stained with basic fuchsine or berberine hemisulfate as described previously (Ursache et al., 2018).

Sections were imaged using an inverted confocal microscope (Leica SP8 or LSM 880; Carl Zeiss), for SCRI Renaissance stain, a 405 laser was used with 1% of laser intensity, 750 gain, 1 AU pinhole diameter and a detection range of 410–502, for berberine stain, a 488 laser was used with 9% of laser intensity, 600 gain, 1 AU pinhole diameter and a detection range of 504–540. For basic fuchsine a 561 laser was used with 2% laser intensity, 700 gain, 1 AU pinhole diameter, and a detection range of 600–650.

Preparation of root extracts and HIFs treatment

Arabidopsis and rice seeds were sterilized, germinated, and grown on half-strength MS medium for 3 weeks. The roots were harvested in liquid nitrogen and grinded. The resulting powder was dissolved in sterile water to a concentration of 5% (w/v) and used to a final concentration of 0.5% in the medium as described previously (Wada et al., 2019).

Striga seeds were germinated in water with GR24 for 24 h, then transferred to a six-well plates containing half-strength MS medium liquid supplemented by either plant root extracts or 10-μM DMBQ.

For plant extracts samples were imaged after 8 h and 12 h and 24 h of treatments. For DMBQ, plants were imaged after 12-h treatments.

Striga imaging was performed using EVOS Cell Imaging System (Thermo Fisher technologies). Quantification of the rate prehaustoria formation was done by counting the number of differentiated striga divided by the total number of germinated ones.

Auxin treatment

Striga hermonthica germination was induced with GR24 for 48 h. Seedlings were then transferred to water containing different concentrations of IAA of 10^{-9}–10^{-5} M. The cell division rate in the meristem was monitored daily for 4 days after IAA treatment.

Treatment with auxin transport and auxin biosynthesis Inhibitors

Striga seeds were germinated in water containing GR24 and 10-μM NPA for 24 h, then transferred to a six-well plates containing half-strength MS medium liquid with and without roots extracts for 12 h.

Inhibition of auxin biosynthesis was performed by transferring germinated striga to six-well plates containing half-strength MS medium liquid supplemented with 1.5-μM L kynurenine. Edu staining, imaging, and counting were done as described above.

RNA in situ hybridization

Striga hermonthica homolog genes were identified by blasting the CDS of Arabidopsis genes at the Parasitic Plant Genome Project website (http://ppgp.huck.psu.edu; Yang et al., 2015). The expressed sequence tags were also blasted to the recently released genome (Yoshida et al., 2019). The

S. hermonthica sequences with the best hit were used for generating and cloning the probes. For RNA probes, cDNA fragments with lengths of 500–1,340 bp were amplified with Phusion polymerase using *S. hermonthica* cDNA obtained from seedlings. The obtained products were cloned into pGEM-T Easy Vector (Promega). The probes were synthesized by amplifying the cloned fragment with M13 primers. The purified product was then used for an in vitro transcription reaction using the DIG RNA Labeling Mix (#11175025910, Roche, Germany) and T7 and Sp6 RNA polymerase to generate both sense and antisense probes. Whole-mount RNA in situ hybridizations were performed in seedlings embedded in low-melting point agarose and sectioned as described previously (Hejátko et al., 2006). The samples were imaged using the transmitted light illumination Leica DM2500 microscope (Leica Microsystems). The sequences of the primers used to obtain the cDNA fragments are listed in Supplemental Table S2.

Immunolocalization

Whole-mount immunolocalization experiments using anti-PIN1 (Gälweiler et al., 1998) and anti-PIN2 (Müller et al., 1998) antibodies were performed as described previously (Blilou et al., 2005). To detect root cap cells with LM8 (Plant probes, PP-008), auxins with anti-IAA (Agrisera product no. AS06 193), and cytokinins with anti-cytokinin (Agrisera product no. AS09 437), immunolocalization was performed on paraffin sections as described previously (Forestan and Varotto, 2013). The antibodies were diluted as follows: 1/1,000 dilution for anti-PIN1 and -PIN2 and 1/500 for LM8, auxins and cytokinins. For secondary antibodies, goat anti-rabbit IgG and Alexa Fluor 488 (ThermoFisher) at a dilution of 1/1,000 were used. Images were acquired using a Leica Sp8 inverted confocal microscope. Confocal settings were described above.

3D time-lapse imaging and quantification of fluorescence intensity

Arabidopsis seedlings containing *DR5::vYFP* and *DII::venus* were grown for 5 days and were put in contact with germinated *S. hermonthica* for 48 h until prehaustorium formation. To acquire time-lapse images in 3D using *DR5::vYFP*, Z-stack images were recorded using Zen software at a rate of 50 frames with 104 slices and an average of 4 frames/s using a 10× plan Apochromat objective lens. To acquire fluorescence time-lapse images of Arabidopsis roots using *DR5::vYFP* and *DII::venus*, the fluorescence was visualized when roots were put in contact with *S. hermonthica* and the signal was recorded daily for 48 h for each root using a Plan-Apochromat 20× objective. YFP was excited at 514 nm, emission was recorded at 519–620 nm, with 7% of laser intensity, 750 gain, 1 AU pinhole diameter. The fluorescence intensity was then quantified using ImageJ software as described previously (Long et al., 2017, 2018).

Phylogenetic analysis and gene IDs

To construct the PIN and PLT phylogenetic tree, the Arabidopsis PIN1 and PLT1 amino acid sequences were used for a BLAST search for homolog sequences in the *Striga asiatica* genome release with a cut-off value of e-value $<2^{e\text{-}05}$ for PIN and $<7^{e\text{-}55}$ for PLT. Arabidopsis PLT sequences were obtained from arabidopsis.org. The sequences were aligned using Muscle in MEGA X (Kumar et al., 2018), and the evolutionary history was inferred using the Maximum Likelihood method and JTT matrix-based model integrated into the software with a bootstrap value of 100.

The following gene IDs are mentioned in this study: *ShPLT1/2* (StHeBC3_20835.1, GER38334), *ShHISTONE H4* (StHe2GB1_80290), *ShCYCLIN B1,3* (StHeBC3_3205), *ShPIN1* (StHe61GB1_24115, GER51912), and *ShPIN2* (GER52036.1).

Statistical analysis

Meristem size measurements and cell number were performed in germinated Striga seeds after 24 and 48 h of GR24. Data are represented as Boxplots. Box limits indicate the 25th and 75th percentiles. Whiskers extend to the 5th and 95th percentiles. All box plots were generated using IBM SPSS Statistics for Windows, version V26.

Accession numbers

The genes used in this study have the following accession numbers: *ShPLT1* (StHeBC3_20835.1; GER38334); *ShHISTONE H4* (StHe2GB1_80290); *ShCYCLIN B1,3* (StHeBC3_3205); *ShPIN1* (StHe61GB1_24115; GER51912); and *ShPIN2* (GER52036.1).

Supplemental data

The following materials are available in the online version of this article.

Supplemental Figure S1. Striga root development.

Supplemental Figure S2. Schematic representation of different stages of Striga root development.

Supplemental Figure S3. Phylogenetic tree of *S. hermonthica* and Arabidopsis PLT proteins.

Supplemental Figure S4. Schematic representation showing cell division rates in Striga roots with and without rice extract.

Supplemental Figure S5. Chemical treatment to induce pre-haustorium formation

Supplemental Figure S6. EdU detection in *S. hermonthica* root tips treated with different molar concentrations of IAA

Supplemental Figure S7. Phylogenetic tree of *S. hermonthica* and Arabidopsis PIN proteins.

Supplemental Figure S8. Immunolocalization assays.

Supplemental Figure S9. *Striga hermonthica* root structure layout used for constructing the mathematical model.

Supplemental Figure S10. Auxin distribution pattern simulated in the mathematical model.

Supplemental Figure S11. Striga increases auxin levels only when a prehaustorium is formed and is in physical contact with Arabidopsis roots.

Supplemental Methods S1. Mathematical modeling.

Supplemental Table S1. Striga prehaustorium formation with MQ, Arabidopsis, rice extracts, DMBQ, and auxin competitive inhibitor L-kynurenine treatment.

Supplemental Table S2. Striga prehaustorium formation with MQ, and rice extracts with and without the auxin transport inhibitor NPA.

Supplemental Table S3. Parameter settings used in the mathematical model.

Supplemental Table S4. Primers used in this study.

Supplemental Movie S1. Time lapse of *S. hermonthica* forming a prehaustoria in contact with Arabidopsis roots containing *DR5::vYFP*.

Supplemental Movie S2. Time lapse of *S. hermonthica* in contact with Arabidopsis roots containing *DR5::vYFP* without forming a prehaustoria.

Supplemental Movie S3. Time lapse of *S. hermonthica* without physical contact with Arabidopsis roots containing *DR5::vYFP*.

Acknowledgments

We thank Prof. Jiri Friml for generously providing AtPIN1 and AtPIN2 antibodies. We thank Dr. Wei Xu for the technical support during confocal imaging.

Funding

This study was supported by King Abdullah University of Science and Technology (KAUST) baseline funding given to Ikram Blilou and by the Bill and Melinda Gates Foundation grant OPP1194472 given to Salim Al-Babili. Realistic root models developed in the frame of Deutsche Forschungsgemeinschaft (DFG, German Research Foundation) and the Russian Foundation for Basic Research (RFBR) joint project RFBR-DFG 19-54-12013. Mathematical modeling was supported by FWNR-2022-0020.

Conflict of interest statement. The authors declare that they have no conflicts of interest.

References

Abas L, Kolb M, Stadlmann J, Janacek DP, Lukic K, Schwechheimer C, A.Sazanov L, Mach L, Friml J, Hammes UZ (2021) Naphthylphthalamic acid associates with and inhibits PIN auxin transporters. Proc Natl Acad Sci USA **118**: e2020857118

Aida M, Beis D, Heidstra R, Willemsen V, Blilou I, Galinha C, Nussaume L, Noh YS, Amasino R, Scheres B (2004) The P LET HORA genes mediate patterning of the Arabidopsis root stem cell niche. Cell **9**: 109–120

Al-Babili S, Bouwmeester HJ (2015) Strigolactones, a novel plant hormone. Annu Rev Plant Biol **66**: 161–186

Albrecht H, Yoder JI, Phillips DA (1999) Flavonoids promote haustoria formation in the root parasite Triphysaria versicolor. Plant Physiol **119**: 585–591

Baird W V., Riopel JL (1983) Experimental studies of the attachment of the parasitic angiosperm Agalinis purpurea to a host. Protoplasma **118**: 206–218

Bengough AG, McKenzie BM (1997) Sloughing of root cap cells decreases the frictional resistance to maize (*Zea mays* L.) root growth. J Exp Bot **48**: 885–893

Van den berg C, Willemsen V, Hendriks G, Weisbeek P, Scheres B (1997) Short-range control of cell differentiation in the Arabidopsis root meristem. Nature **390**: 287–289

Blilou I, Xu J, Wildwater M, Willemsen V, Paponov I, Friml J, Heidstra R, Aida M, Palme K, Scheres B (2005) The PIN auxin efflux facilitator network controls growth and patterning in *Arabidopsis* roots. Nature **433**: 39–44

Bulankova P, Akimcheva S, Fellner N, Riha K (2013) Identification of Arabidopsis meiotic cyclins reveals functional diversification among plant cyclin genes. PLoS Genet **9**: e1003508

Chaimovitsh D, Rogovoy Stelmakh O, Altshuler O, Belausov E, Abu-Abied M, Rubin B, Sadot E, Dudai N (2012) The relative effect of citral on mitotic microtubules in wheat roots and BY2 cells. Plant Biol **14**: 354–364

Chang M, Lynn DG (1986) The haustorium and the chemistry of host recognition in parasitic angiosperms. J Chem Ecol **12**: 561–579

Chang M, Netzly DH, Butler LH, Lynn DG (1986) Chemical regulation of distance: characterization of the first natural host germination stimulant for Striga asiatica. J Am Chem Soc **108**: 7858–7860

Cook CE, Whichard LP, Wall ME, Egley GH, Coggon P, Luhan PA, Mcphail AT (1972) Germination stimulants. II. The structure of strigol–A potent seed germination stimulant for witchweed (Striga lutea Lour.)1,2. J Am Chem Soc **94**: 6198–6199

Cruz-Ramírez A, Díaz-Triviño S, Wachsman G, Du Y, Arteága-Vázquez M, Zhang H, Benjamins R, Blilou I, Neef AB, Chandler V, et al. (2013) A SCARECROW-RETINOBLASTOMA protein network controls protective quiescence in the Arabidopsis root stem cell organizer. PLoS Biol

Cui S, Wada S, Tobimatsu Y, Takeda Y, Saucet SB, Takano T, Umezawa T, Shirasu K, Yoshida S (2018) Host lignin composition affects haustorium induction in the parasitic plants Phtheirospermum japonicum and Striga hermonthica. New Phytol **218**: 710–723

Dastidar MG, Scarpa A, Mägele I, Ruiz-Duarte P, von Born P, Bald L, Jouannet V, Maizel A (2019) ARF5/MONOPTEROS directly regulates miR390 expression in the Arabidopsis thaliana primary root meristem. Plant Direct 3: e00116

Ejeta G (2007) The Striga scourge in Africa: a growing pandemic. *In* G Ejeta, J Gressel, eds, Integrating New Technologies for Striga Control Towards Ending the Witch-hunt. World Scientific Publishing Co. Pte. Ltd, Singapore, pp 3–16

Forestan C, Varotto S (2013) Auxin immunolocalization in plant tissues. Methods Mol Biol **959**: 223–233

Furuta KM, Xiang L, Cui S, Yoshida S (2021) Molecular dissection of haustorium development in Orobanchaceae parasitic plants. Plant Physiol **186**: 1424–1434

Galinha C, Hofhuis H, Luijten M, Willemsen V, Blilou I, Heidstra R, Scheres B (2007) PLETHORA proteins as dose-dependent master regulators of Arabidopsis root development. Nature **449**: 1053–1057

Gälweiler L, Guan C, Müller A, Wisman E, Mendgen K, Yephremov A, Palme K (1998) Regulation of polar auxin transport by AtPIN1 in Arabidopsis vascular tissue. Science **282**: 2226–2230

Goyet V, Wada S, Cui S, Wakatake T, Shirasu K, Montiel G, Simier P, Yoshida S (2019) Haustorium inducing factors for parasitic Orobanchaceae. Front Plant Sci **10**: 1–8

Grieneisen VA, Xu J, Marée AFM, Hogeweg P, Scheres B (2007) Auxin transport is sufficient to generate a maximum and gradient guiding root growth. Nature **449**: 1008–1013

Gutierrez C (2009) The Arabidopsis cell division cycle. The Arabidopsis Book **7**: e0120

He W, Brumos J, Li H, Ji Y, Ke M, Gong X, Zeng Q, Li W, Zhang X, An F, et al. (2011) A small-molecule screen identifies L-kynurenine as a competitive inhibitor of TAA1/TAR activity in ethylene-directed auxin biosynthesis and root growth in Arabidopsis. Plant Cell **23**: 3944–3960

Hejátko J, Blilou I, Brewer PB, Friml J, Scheres B, Benková E (2006) In situ hybridization technique for mRNA detection in whole mount Arabidopsis samples. Nat Protoc **1**: 1939–1946

Hood ME, Condon JM, Timko MP, Riopel JL (1998) Primary haustorial development of striga asiatica on host and nonhost species. Genet Resist **88**: 70–75

Dello Ioio R, Nakamura K, Moubayidin L, Perilli S, Taniguchi M, Morita MT, Aoyama T, Costantino P, Sabatini S (2008) A genetic framework for the control of cell division and differentiation in the root meristem. Science **322**: 1380–1384

Ishida JK, Wakatake T, Yoshida S, Takebayashi Y, Kasahara H, Wafula E, Depamphilis CW, Namba S, Shirasu K (2016) Local auxin biosynthesis mediated by a yucca flavin monooxygenase regulates haustorium development in the parasitic plant phtheirospermum japonicum. Plant Cell **28**: 1795–1814

Ivanchenko MG, Zhu J, Wang B, Medvecká E, Du Y, Azzarello E, Mancuso S, Megraw M, Filichkin S, Dubrovsky JG, et al. (2015) The cyclophilin a DIAGEOTROPICA gene affects auxin transport in both root and shoot to control lateral root formation. Dev **142**: 712–721

Joel DM, Gressel J, Musselman LJ (2013) Parasitic Orobanchaceae. Parasitic mechanisms and control strategies. New York

Joel DM (2013) The haustorium and the life cycles of parasitic Orobanchaceae. *In* DM Joel, J Gressel, LJ Musselman, eds, Parasitic Orobanchaceae. Springer, New York, pp 21–24

Joel DM, Losner-Goshen D (1994) The attachment organ of the parasitic angiosperms Orobanche cumana and O. aegyptiaca and its development. Can J Bot **72**: 564–574

Kaštier P, Krasylenko YA, Martinčová M, Panteris E, Šamaj J, Blehová A (2018) Cytoskeleton in the parasitic plant cuscuta during germination and prehaustorium formation. Front Plant Sci **9**: 1–17

Keyes WJ, Taylor J V., Apkarian RP, Lynn DG (2001) Dancing together. Social controls in parasitic plant development. Plant Physiol **127**: 1508–1512

Kirschner GK, Stahl Y, Von Korff M, Simon R (2017) Unique and conserved features of the barley root meristem. Front Plant Sci **8**: 1240

Kountche BA, Al-Babili S, Haussmann B (2016) Striga: a persistent problem on millets. *In* IK Das, PG Padmaja, eds, Biotic Stress Resistance in Millets. Academic Press, pp 173–203

Kountche BA, Jamil M, Yonli D, Nikiema MP, Blanco-Ania D, Asami T, Zwanenburg B, Al-Babili S (2019) Suicidal germination as a control strategy for Striga hermonthica (Benth.) in smallholder farms of sub-Saharan Africa. Plants, People, Planet **1**: 107–118

Kumar S, Stecher G, Li M, Knyaz C, Tamura K (2018) MEGA X: molecular evolutionary genetics analysis across computing platforms. Mol Biol Evol **35**: 1547–1549

Kumpf RP, Nowack MK (2015) The root cap: a short story of life and death. J Exp Bot **66**: 5651–5662

Kyndt T, Goverse A, Haegeman A, Warmerdam S, Wanjau C, Jahani M, Engler G, De Almeida Engler J, Gheysen G (2016) Redirection of auxin flow in Arabidopsis thaliana roots after infection by root-knot nematodes. J Exp Bot **67**: 4559–4570

Laohavisit A, Wakatake T, Ishihama N, Mulvey H, Takizawa K, Suzuki T, Shirasu K (2020) Quinone perception in plants via leucine-rich-repeat receptor-like kinases. Nature **587**: 92–97

Lee BH, Johnston R, Yang Y, Gallavotti A, Kojima M, Travençolo BAN, Costa LDF, Sakakibara H, Jackson D (2009) Studies of aberrant phyllotaxy1 mutants of maize indicate complex interactions between auxin and cytokinin signaling in the shoot apical meristem 1[W][OA]. Plant Physiol **150**: 205–216

Lee Y (2019) Redox control on stem cell fate and maintenance in the root. J Plant Biol **62**: 320–328

Long Y, Stahl Y, Weidtkamp-Peters S, Postma M, Zhou W, Goedhart J, Sánchez-Pérez M-I, Gadella TWJ, Simon R, Scheres B, et al. (2017) In vivo FRET–FLIM reveals cell-type-specific protein interactions in Arabidopsis roots. Nature **548**: 97–102

Long Y, Stahl Y, Weidtkamp-peters S, Smet W, Du Y, Gadella TWJ, Goedhart, Joachim, Scheres, Ben, Blilou I (2018) Optimizing FRET-FLIM labeling conditions to detect nuclear protein interactions at native expression levels in living Arabidopsis roots. Front Plant Sci **9**: 639

Mähönen AP, Tusscher K, Siligato R, Smetana O (2014) PLETHORA gradient formation mechanism separates auxin responses. Nature **515**: 125–129

Majda M, Robert S (2018) The role of auxin in cell wall expansion. Int J Mol Sci **19**: 951

Moubayidin L, Perilli S, Dello Ioio R, Di Mambro R, Costantino P, Sabatini S (2010) The rate of cell differentiation controls the Arabidopsis root meristem growth phase. Curr Biol **20**: 1138–1143

Mravec J, Kračun SK, Zemlyanskaya E, Rydahl MG, Guo X, Pičmanová M, Sørensen KK, Růžička K, Willats WGT (2017) Click chemistry-based tracking reveals putative cell wall-located auxin binding sites in expanding cells. Sci Rep **7**: 1–13

Müller A, Guan C, Ta P, Huijser P, Marchant A, Parry G, Bennett M, Wisman E, Palme K (1998) AtPIN2 defines a locus of Arabidopsis for root gravitropism control. EMBO J **17**: 6903–6911

Musielak TJ, Schenkel L, Kolb M, Henschen A, Bayer M (2015) A simple and versatile cell wall staining protocol to study plant reproduction. Plant Reprod **28**: 161–169

Okonkwo SNC, Raghavan V (1982) Studies on the germination of seeds of the root parasites, Alectra vogelii and Striga gesnerioides. I. Anatomical changes in the embryos. Am J Bot **69**: 1636–1645

Pasternak T, Tietz O, Rapp K, Begheldo M, Nitschke R, Ruperti B, Palme K (2015) Protocol: an improved and universal procedure for whole-mount immunolocalization in plants. Plant Methods **11**: 1–11

Pennisi E (2015) How crop-killing witchweed senses its victims. Science **350**: 146–147

Perez-de-Luque A (2013) Haustorium invasion into host tissues. *In* DM Joel, J Gressel, J Musselman, eds, Parasitic Orobanchaceae. Springer, Heidelberg, pp 75–86

Raghavan V, Okonkwo SN (1982) Studies on the germination of seeds of the root parasites, Alectra vogelii and Striga gesnerioides. II. DNA synthesis and development of the quiescent center in the radicle. Am J Bot **69**: 1646–1656

Ranjan A, Ichihashi Y, Farhi M, Zumstein K, Townsley B, David-Schwartz R, Sinha NR (2014) De novo assembly and characterization of the transcriptome of the parasitic weed dodder identifies genes associated with plant parasitism. Plant Physiol **166**: 1186–1199

Reiss GC, Bailey JA (1998) Striga gesnerioides parasitising cowpea: development of infection structures and mechanisms of penetration. Ann Bot **81**: 431–440

Sabatini S, Beis D, Wolkenfelt H, Murfett J, Guilfoyle T, Malamy J, Benfey P, Leyser O, Bechtold N, Weisbeek P, et al. (1999) An auxin-dependent distal organizer of pattern and polarity in the Arabidopsis root. Cell **99**: 463–472

Savina MS, Mironova VV (2020) Plant layout pipeline to model tissue patterning. Vavilovskii Zhurnal Genet Selektsii **24**: 102–107

Tomilov AA, Tomilova NB, Abdallah I, Yoder JI (2005) Localized hormone fluxes and early haustorium development in the hemiparasitic plant Triphysaria versicolor. Plant Physiol **138**: 1469–1480

Torres MJ, Tomilov AA, Tomilova N, Reagan RL, Yoder JI (2005) Pscroph, a parasitic plant EST database enriched for parasite associated transcripts. BMC Plant Biol **5**: 1–9

Truernit E, Bauby H, Dubreucq B, Grandjean O, Runions J, Barthélémy J, Palauqui J-C (2008) High-resolution whole-mount imaging of three-dimensional tissue organization and gene expression enables the study of Phloem development and structure in Arabidopsis. Plant Cell **20**: 1494–1503

Ursache R, Andersen TG, Marhavý P, Geldner N (2018) A protocol for combining fluorescent proteins with histological stains for diverse cell wall components. Plant J **93**: 399–412

Vieten A, Vanneste S, Wiśniewska J, Benková E, Benjamins R, Beeckman T, Luschnig C, Friml J (2005) Functional redundancy

of PIN proteins is accompanied by auxin-dependent cross-regulation of PIN expression. Development **132**: 4521–4531

Wada S, Cui S, Yoshida S (2019) Reactive oxygen species (ROS) generation is indispensable for haustorium formation of the root parasitic plant striga hermonthica. Front Plant Sci **10**: 1–12

Wakatake T, Ogawa S, Yoshida S, Shirasu K (2020) An auxin transport network underlies xylem bridge formation between the hemi-parasitic plant Phtheirospermum japonicum and host Arabidopsis. Development. Doi: 10.1242/dev.187781

Westwood JH, Yoder JI, Timko MP, dePamphilis CW (2010) The evolution of parasitism in plants. Trends Plant Sci **15**: 227–235

Willats WGT, McCartney L, Steele-King CG, Marcus SE, Mort A, Huisman M, Van Alebeek GJ, Schols HA, Voragen AGJ, Le Goff A, et al. (2004) A xylogalacturonan epitope is specifically associated with plant cell detachment. Planta **218**: 673–681

Wisniewska J, Xu J, Seifartová D, Brewer PB, Růžička K, Blilou L, Rouquié D, Benková E, Scheres B, Friml J (2006) Polar PIN localization directs auxin flow in plants. Science **312**: 883

Woo HH, Jeong BR, Hawes MC (2005) Flavonoids: from cell cycle regulation to biotechnology. Biotechnol Lett **27**: 365–374

Xiao TT, Raygoza AA, Pérez JC, Kirschner G, Deng Y, Atkinson B, Sturrock C, Lube V, Wang JY, Lubineau G, et al. (2019) Emergent protective organogenesis in date palms: a morpho-devo-dynamic adaptive strategy during early development. Plant Cell **31**: 1751–1766

Yamada M, Han X, Benfey PN (2020) RGF1 controls root meristem size through ROS signalling. Nature **577**: 85–88

Yang Z, Wafula EK, Honaas LA, Zhang H, Das M, Fernandez-Aparicio M, Huang K, Bandaranayake PCG, Wu B, Der JP, et al. (2015) Comparative transcriptome analyses reveal core parasitism genes and suggest gene duplication and repurposing as sources of structural novelty. Mol Biol Evol **32**: 767–790

Yoshida S, Cui S, Ichihashi Y, Shirasu K (2016) The haustorium, a specialized invasive organ in parasitic plants. Annu Rev Plant Biol **67**: 643–667

Yoshida S, Kim S, Wafula E, Tanskanen J, Kim Y-M, Shirasu K (2019) Genome sequence of Striga asiatica provides insight into the evolution of plant parasitism. Curr Biol **29**: R868–R871

Zhang W, Swarup R, Bennett M, Schaller GE, Kieber JJ (2013) Cytokinin induces cell division in the quiescent center of the Arabidopsis root apical meristem. Curr Biol **23**: 1979–1989

Zhou W, Lozano-Torres JL, Blilou I, Zhang X, Zhai Q, Smant G, Li C, Scheres B (2019) A jasmonate signaling network activates root stem cells and promotes regeneration. Cell **177**: 942–956.e14